High-temperature viscoelasticity and heat-setting of poly(ethylene terephthalate)*

C. P. Buckley
Department of Mechanical Engineering, UMIST, Manchester M60 1QD, UK

and D. R. Salem
Textile Research Institute, PO Box 625, Princeton, New Jersey 08450, USA
(Received 31 December 1985; revised 27 June 1986)

Viscoelasticity of semicrystalline drawn filaments of poly(ethylene terephthalate) was studied in the temperature range critical in forming processes: between the glass transition and melting regions. Measurements were made of strain recovery following heat-setting in torsion. Microstructural features were also monitored, by density measurement and X-ray scattering. Heat-treated specimens were found to exhibit *two* distinct heat-setting processes. One corresponded to the glass transition. The other was situated between the glass transition and melting regions. This second process has been compared with predictions for heat-setting due to (a) melting/recrystallization, (b) viscous flow. The mechanism is deduced as being viscous flow, corresponding to mechanical relaxation – an α'-relaxation – separate from the glass transition, and probably arising from entanglement slippage. On heat-treatment, the dominant α'-relaxation time at the temperature of treatment was found consistently to increase to approximately equal the time allowed for heat-treatment. This indicates a link between the molecular diffusion processes responsible for α' stress relaxation and those involved in evolution of microstructure and properties during heat-treatment. The magnitude of the α'-relaxation showed increases with increasing time, but decreases with increasing temperature of pre-treatment above 200°C. These are explicable in terms of microstructural changes by using a simple quantitative model for calculating the effective cross-link density of the non-crystalline matrix provided by crystals.

(Keywords: poly(ethylene terephthalate); heat-setting; viscoelasticity; relaxation; drawn fibres)

INTRODUCTION

Forming processes for polymers consist of three basic steps, occurring in the order:

(A) deformation of the polymer while soft;
(B) hardening of the polymer in deformed state;
(C) release of the polymer when hard.

The key to the success of this sequence is the 'fading memory' viscoelastic character of the materials. Briefly, the material's 'memory' of deformation induced at (A) must be faded at least partially before release takes place at (C); otherwise the original shape would be completely recovered. For thermoplastic polymers, of course, the softening required at (A) is usually induced by a rise in temperature, and the hardening required at (B) by a fall in temperature. Example processes are flow followed by solidification in injection moulds, vacuum forming of sheet materials, heat-setting of fibres and fabrics.

In spite of the enormous practical importance of forming processes in manufacturing, there is little information yet available on the crucial viscoelastic behaviour of polymers during the softening and hardening stages involved in forming. This is a serious gap in knowledge, which hinders accurate prediction of material behaviour during forming, and hence represents a source of uncertainty in the design of both processes and materials. The problem is especially acute for semicrystalline polymers. For them, one can envisage at least two alternative possibilities. On the one hand, the primary softening and hardening processes could correspond to temperature-induced acceleration and deceleration of viscous flow, as in wholly amorphous polymers; on the other, they could correspond to melting and crystallization, as in the casting of highly crystalline materials. The latter possibility, if at all applicable to polymers, is most likely to apply to the highly crystalline polymers such as linear polyethylene, isotactic polypropylene and polyoxymethylene. For polymers of lower crystallinity, however, it is not known which of these two possibilities, and indeed others, applies. The work described here was aimed at resolving precisely this issue, for a semicrystalline polymer of great practical importance: poly(ethylene terephthalate) (PET).

As will emerge below, experiments showed viscoelasticity of PET under conditions relevant to forming to be governed not only by the glass transition but also by another, hitherto unsuspected, mechanical relaxation process. It is located between the glass transition and melting regions, but appears to be quite separate from both. We have labelled it the α'-relaxation, to distinguish it from the glass transition (α-relaxation) in PET. The latter part of the paper gives an account of the characteristic features of the α'-relaxation, and how they are related to microstructural changes, and a tentative suggestion for its origin.

* An abbreviated version of this paper was presented at the Fifth International Conference on Deformation, Yield and Fracture of Polymers, held at Cambridge, UK, April 1982.

0032-3861/87/010069-17$3.00

HEAT SETTING

Background

The mechanical tests employed in the present work took the rather unconventional form of 'heat-setting' experiments. We begin by giving reasons for this, and then derive some analytical relations to assist in the interpretation of results.

The temperature region of greatest interest in relation to the forming of PET lies between the glass transition and equilibrium melting point. Here, however, one is faced with a major experimental problem: the PET microstructure is unstable and continuously evolving. There are significant changes in degree of crystallinity and other morphological parameters, and in oriented samples these are accompanied by changes in molecular orientation.

The physical processes involved have been studied extensively[1-26]. In parallel, physical properties are also evolving; these changes too have received much attention[15,27-41].

In such circumstances the experimenter faces a dilemma. If a single specimen is used for a sequence of property measurements, each measurement refers to a different structural state, since the specimen microstructure is evolving during the course of the experiment; this can lead to very misleading results[42]. Experimental artefacts can be avoided only by carefully restricting measurements to temperatures where the microstructure does not change significantly on the timescale of the experiment. In practice, this means making measurements only at temperatures below those where the specimen has previously been heat-treated[42]. Thus, Illers and Breuer[32] in their early, but comprehensive, study of viscoelasticity of PET were careful to restrict their data-gathering in this way. For specimens heat-treated near the glass transition or not far above, therefore, a large portion of the glass transition to melting-point temperature range was inaccessible. Other authors, notably Dumbleton and Murayama[35,37], and more recently Valk *et al.*[38] and Gupta and Kumar[41] have included dynamic mechanical measurements on unannealed or low-temperature annealed PET specimens, up to temperatures approaching the melting region, where microstructural evolution was certain to occur during testing; consequently, those results should be considered unreliable. For example, the doublet structure that was observed in the α-relaxation of cold-drawn unannealed PET[38] is almost certainly an experimental artefact due to annealing of the specimen during testing. It is now clear why there is a shortage of reliable information on the viscoelastic deformation of PET at the temperatures of interest, between the glass transition and melting regions: a radically different experimental method is needed. The method adopted in this work was that of the 'heat-setting' experiment, in which each specimen is

(a) deformed and heated,
(b) cooled,
(c) released.

The parameter measured is the 'fractional recovery' f (the fraction of strain introduced that is recovered on release). A new specimen is used for each data point, so one can be certain of the precise thermal history to which each data point corresponds. It follows that, to avoid ambiguity in interpretation, the specimen must be sufficiently thin that temperature equilibration occurs rapidly and all parts of the specimen receive essentially the same thermal history. We achieved this by using PET specimens in the form of filaments less than 100 μm in diameter.

A further advantage of the heat-setting experiment is that it models in the laboratory a typical forming operation for a thermoplastic polymer, and therefore produces results more practically relevant to forming. This can be seen by comparing (a) to (c) above with (A) to (C) in the previous section. In the present work, the fibre specimens used were cut from drawn samples of PET monofilament yarn. The experiments were designed to be most relevant to the heat-setting of PET yarns and fabrics, forming operations widely used in the textile industry.

Heat-setting experiments of this type have been made previously on drawn PET filaments, in various modes of deformation. Lunn *et al.*[43] and Shishoo and Bergh[44] studied extension, Buckley *et al.*[45] studied torsion, and Arghyros and Backer[46] studied both torsion and bending. The two main results to emerge so far are as follows: fractional recovery decreases with increasing setting temperature[43-46] and increasing strain level[43,45,46]. These results are consistent with the generally observed trends in temperature-dependent nonlinear viscoelasticity of polymers. However, they do not offer insight into the mechanisms contributing to setting at a quantitative level: this was the intention of the present work.

Analysis

It is clear from above that an essential feature of heat-setting is that temperature is varied while the specimen is under load. This will inevitably lead to *changes in properties while the specimen is under load.* If the material is linear viscoelastic, the appropriate form of the Boltzmann superposition principle, giving the stress $\sigma(t)$ at time t in response to a strain history $\gamma(u)$ in one dimension, is

$$\sigma(t)=\int_0^t G_e(t-u,u)(\mathrm{d}\gamma/\mathrm{d}u)\mathrm{d}u+\sigma'_e(t) \qquad (1)$$

$G_e(t-u,u)$ is the effective stress-relaxation modulus for a strain applied at time u followed by stress relaxation until time t: the subscript 'e' indicates that G_e depends on the environmental history up to time t, following Chapman[47]. The additional stress $\sigma'_e(t)$ is the background stress resulting purely from the environmental history in the absence of strain, and the prior strain history.

The heat-setting experiment is shown schematically in *Figure 1*. Strain γ_0 is inserted rapidly at zero time and temperature T_0. At time t_A, the temperature is raised rapidly to the setting temperature T_s. After the setting time t_s, temperature is returned rapidly to T_0. At time t_C the stress σ is released and the strain γ recovers back towards zero. At a later time, the recovered strain γ_r is measured. Applying equation (1) to this sequence, we obtain the following integral equation for the fractional recovery $f=\gamma_r/\gamma_0$ at time $u>t_C$

$$\int_{t_C}^{t} G_e(t-u,u)\frac{\mathrm{d}f}{\mathrm{d}u}\mathrm{d}u=G_e(t,0)+\frac{\sigma'_e(t)}{\gamma_0} \qquad (2)$$

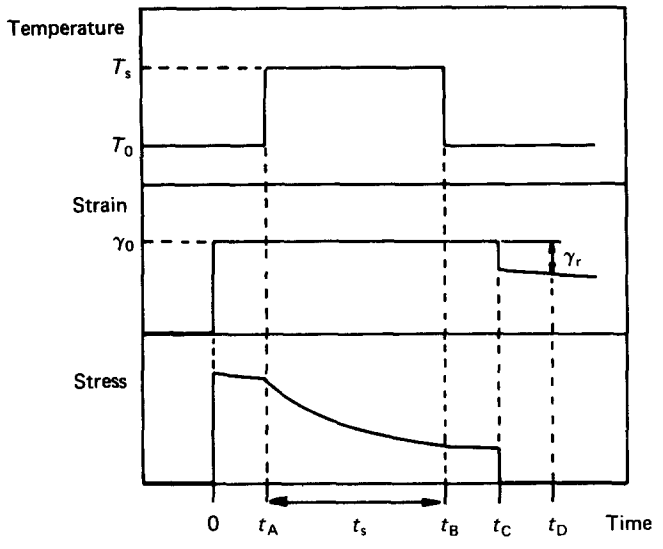

Figure 1 Schematic diagram of the heat-setting experiment

In the present work, the background stress σ_e' could be neglected to a reasonable approximation since the mode of deformation was torsion (see later). Moreover, the material studied was PET and the temperature T_0 was chosen to be 20°C, where viscoelasticity in this material is not severe. Under these conditions, as discussed by Denby[48], equation (2) can be solved to a good approximation to yield the recovery at time t:

$$f(t)=\frac{G_e(t,0)}{G_e(t-t_C,t_C)} \qquad (t>t_C) \tag{3}$$

Note that equation (3) is *not* restricted to a material whose properties are constant with time. For example, it has been applied successfully to setting of wool fabrics under varying temperature and humidity[49]: a system in which pronounced ageing effects occur.

Our objective is to identify the mechanism(s) by which heat-setting occurs at forming temperatures in PET. The two main candidates for consideration are: (1) viscous flow, and (2) melting/recrystallization. An essential first step is to predict the pattern of heat-setting behaviour each mechanism would yield, so that they can be compared critically with experimental data.

Heat-setting by viscous flow

Let the normalized distribution of relaxation times τ be $\phi(\tau)$, and the unrelaxed modulus G_u, following the nomenclature of McCrum, Read and Williams[50]. There is no relaxed modulus if the material is a viscoelastic *fluid* and so is capable of viscous flow and of being permanently set into a new shape. Hence the isothermal stress relaxation modulus for a specimen with constant properties is

$$G(t)=G_u\int_{-\infty}^{\infty}\phi(\tau)\exp(-t/\tau)\mathrm{d}\ln\tau \tag{4}$$

To simplify the prediction of response to varying temperature, assume the material is 'thermorheologically simple', i.e. the effect of varying temperature is only to uniformly accelerate or decelerate all viscoelastic functions. This is a reasonable description of the behaviour of PET in the glass transition region for example[51]. The most convenient means of expressing such behaviour is to employ the 'equivalent time' ζ introduced by Morland and Lee[52] which is the time that would produce the same response under isothermal conditions at some reference temperature T^*, as is produced under varying temperature at the real time t. Then, if ϕ^* is the normalized distribution of relaxation times at temperature T^*, the environment-dependent stress-relaxation modulus for a strain applied at time u (equivalent time ζ') followed by stress relaxation until time t (equivalent time ζ) is given by

$$G_e(t-u,u)=G_u\int_{-\infty}^{\infty}\phi^*(\tau)\exp[-(\zeta-\zeta')/\tau]\mathrm{d}\ln\tau \tag{5}$$

where ζ and ζ' are expressed in terms of the time–temperature shift factor a_T as follows

$$\zeta=\int_0^t\frac{\mathrm{d}t'}{a_T} \qquad \zeta'=\int_0^u\frac{\mathrm{d}t'}{a_T} \tag{6}$$

for a temperature–time sequence $T(t')$.

A convenient way of representing the expansion and contraction of timescale implied by use of the equivalent-time concept is the *equivalent-time/real-time diagram*. The path of any given temperature history can be mapped onto this diagram by noting that at any instant its gradient is given by

$$\frac{\mathrm{d}\zeta}{\mathrm{d}t}=\frac{1}{a_T} \tag{7}$$

For the heat-setting experiment of *Figure 1*, this diagram takes the form shown schematically in *Figure 2*. For practical purposes we can neglect the contribution to stress relaxation occurring at 20°C compared to that occurring at the setting temperature t_s, i.e. we can assume $a_{T_s} \ll a_{T_0}$ (see *Figure 2*). With this approximation, equation

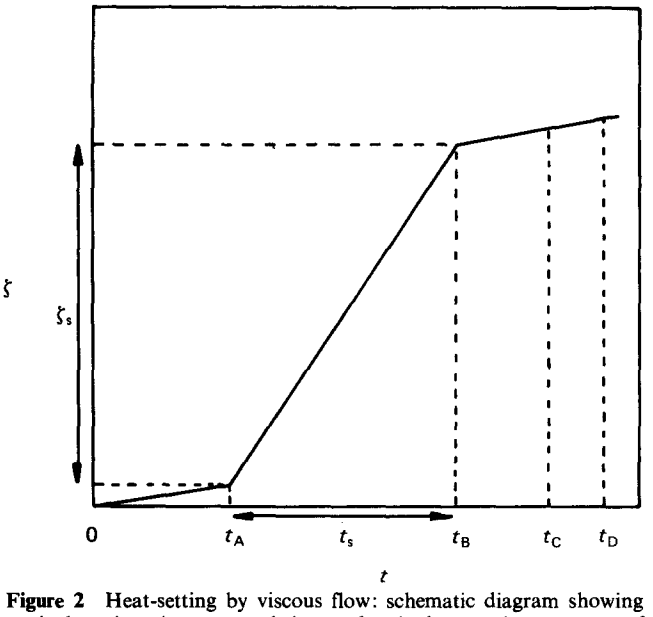

Figure 2 Heat-setting by viscous flow: schematic diagram showing equivalent time, ζ, *versus* real time, t, for the heat-setting sequence of *Figure* 1 ($\zeta_s=t_s/a_{T_s}$; see text)

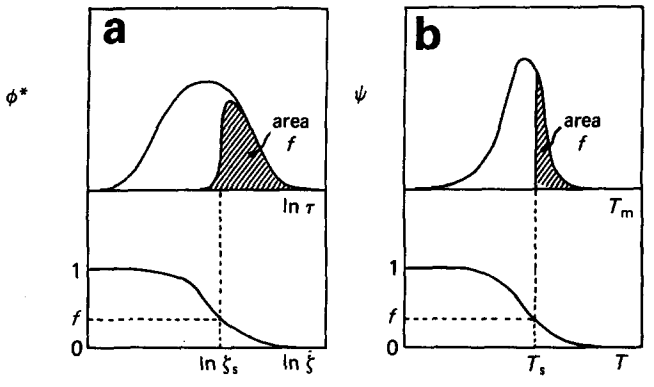

Figure 3 Schematic diagrams showing the relations between fractional recovery, f, and relaxation spectrum, $\phi^*(\tau)$, or melting spectrum, $\psi(T_m)$, according to the two mechanisms: (a) heat-setting by viscous flow; (b) heat-setting by melting/recrystallization

(5) yields for $t > t_C$:

$$G_e(t,0) = G_u \int_{-\infty}^{\infty} \phi^*(\tau)\exp(-\zeta_s/\tau)\, d\ln\tau$$
$$G_e(t - t_C, t_C) = G_u \tag{7}$$

where $\zeta_s = t_s/a_{T_s}$.

Substituting into equation (3) we obtain a prediction of the fractional recovery

$$f = \int_{-\infty}^{\infty} \phi^*(\tau)\exp(-\zeta_s/\tau)\, d\ln\tau \tag{8}$$

The relation between f and ϕ^* given by equation (8) is shown in the sketch of *Figure 3a*. Furthermore, the approximation suggested by Alfrey and Doty[53] may be applied to equation (8) to yield

$$\phi^*(\tau) \simeq \left.\frac{-df}{d\ln\zeta_s}\right|_{\zeta_s=\tau} \tag{9}$$

For heat-setting experiments made at constant t_s or T_s equation (9) then gives, respectively,

$$\phi^*(\tau) \simeq \left.\frac{-df}{dT_s}\left(-\frac{dT_s}{d\ln a_{T_s}}\right)\right|_{a_{T_s}=t_s/\tau} \tag{10a}$$

$$\phi^*(\tau) \simeq -\left.\frac{df}{d\ln t_s}\right|_{t_s=\tau a_{T_s}} \tag{10b}$$

Equations (10a, b) allow measurements of f to be interpreted in terms of the distribution of relaxation times $\phi^*(\tau)$, if heat-setting occurs by the viscous flow mechanism.

Heat-setting by melting/recrystallization

It has been widely assumed in the past that heat-setting of semicrystalline polymers near the melting region occurs by a combination of partial melting and recrystallization. Lower-melting, less stable, crystals are imagined to melt while the material is in the deformed state. Recrystallization at the setting temperature and during cooling then stabilizes the new shape before stress is released[54]. Such a mechanism seems very plausible for polymers, in view of their broad melting ranges, but does not appear to have been rigorously tested. To do so, it is first necessary to put the hypothesis into a precise quantitative form. According to the melting/recrystallization hypothesis, crystals prevent flow by providing a continuous elastic network. A possible mechanism would be by the crystals acting as 'cross-links', in the manner shown in *Figure 4a*. At high temperatures, above the glass-transition temperature, the modulus is expected to be highly sensitive to the rigidity of the network: a precise model is suggested later. At a temperature in the melting region the modulus is reduced as crystals melt, and is then recovered again during re-crystallization at this temperature and during subsequent cooling. In terms of the 'cross-linking' action of crystals, melting corresponds to dissolution of cross-links and re-crystallization to their re-formation. The significant point, however, is that *during heat-setting recrystallization occurs with the deformed state as the stress-free state*, i.e. the material loses its 'memory' of the prior deformation: this is why a set is achieved.

The mechanical hysteresis introduced by melting and re-crystallization has the following characteristic features: (1) at temperatures below the melting point the material is elastic; (2) at temperatures above the melting point the material can carry no stress (we ignore here the melt viscosity); (3) passage downwards in temperature through the melting point establishes a new equilibrium (zero stress) size and shape of specimen at the values existing as the melting point is passed (we ignore here thermal expansion and the temperature difference between melting and crystallization).

Such behaviour can be represented symbolically by the simple spring/switch element shown in *Figure 4b*. The spring is of stiffness G_u and the switch has an associated critical temperature T_m, such that it is open at temperatures above T_m and closed at temperatures below T_m. T_m may be identified with the temperatures of melting

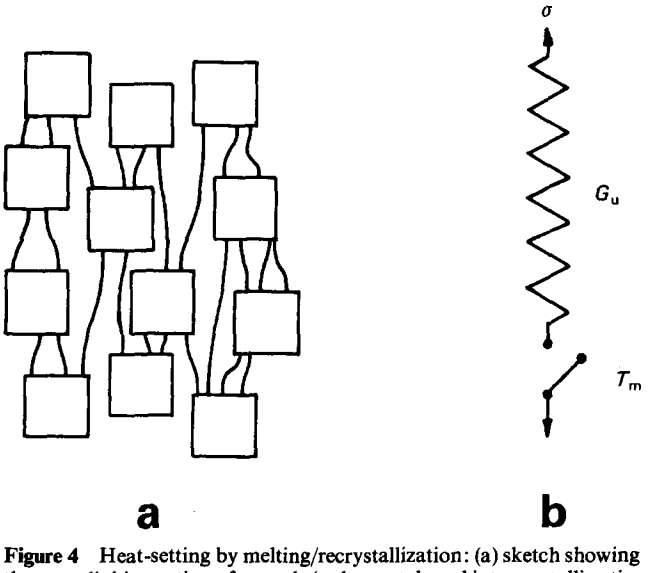

Figure 4 Heat-setting by melting/recrystallization: (a) sketch showing the cross-linking action of crystals (only crystals and intercrystalline tie-segments are shown); (b) simple mechanical model for melting/recrystallization. For $T < T_m$ the switch is closed since crystals act as cross-links (as in (a)); for $T > T_m$ the switch is open since crystals have melted

and crystallization (assumed for present purposes to be equal). The response of the element is as follows at temperature T:

$$\left.\begin{array}{ll} T > T_m & \sigma(t) = 0 \\ T < T_m & \sigma(t) = [\gamma(t) - \gamma(u_l)]G_u \end{array}\right\} \quad (11)$$

where u_l is the time at which the temperature last passed through T_m. So, for an element of strain $\delta\gamma(u)$ applied at time u, the stress resulting at time t is either (a) zero, or (b) $G_u\delta\gamma$, depending on whether or not the switch has opened since it was applied, i.e. whether the maximum temperature $\hat{T}(t,u)$ reached during the time interval u to t was greater or less than T_m. This can be expressed

$$\delta\sigma(t) = G_u h(T_m - \hat{T}(t,u))\delta\gamma(u) \quad (12)$$

where $h(x)$ is the Heaviside unit step function

$$\left.\begin{array}{ll} h(x) = 0 & x \leqslant 0 \\ h(x) = 1 & x > 0 \end{array}\right\} \quad (13)$$

Integrating equation (12) over all parts of the strain history, we obtain the total stress at time t

$$\sigma(t) = \int_0^t G_u h(T_m - \hat{T}(t,u))(\mathrm{d}\gamma/\mathrm{d}u)\mathrm{d}u \quad (14)$$

By comparison with equation (1) we see that the model implies

$$G_e(t-u,u) = G_u h(T_m - \hat{T}(t,u)) \quad (15)$$

The single spring/switch element is clearly insufficient to model heat-setting fully: it predicts only no set ($f=1$) if no melting occurs, or complete set ($f=0$) if melting occurs, and precludes the more usual case of partial set (fractional f).

It is straightforward to extend the model to include the possibility of partial set, by allowing for a range of melting temperatures T_m. The stress will have contributions from crystals covering the entire melting range. Let $\psi(T_m)$ be a normalized distribution of melting points, such that $\psi(T_m)\mathrm{d}T_m$ is the fraction of the unrelaxed modulus contributed by crystals with melting points in the range T_m to $T_m + \mathrm{d}T_m$. By integrating over all possible melting temperatures we can then generalize equation (15) to obtain

$$G_e(t-u,u) = G_u \int_0^{T_m^0} \psi(T_m) h(T_m - \hat{T}(t,u))\mathrm{d}T_m \quad (16)$$

where the upper limit on T_m, T_m^0 is the thermodynamic equilibrium melting point for the polymer.

Equation (16) may be applied to the heat-setting experiment of *Figure 1*, giving

$$\left.\begin{array}{l} G_e(t,0) = G_u \displaystyle\int_{T_s}^{T_m^0} \psi(T_m)\mathrm{d}T_m \\ G_e(t-t_C,t_C) = G_u \end{array}\right\} \quad (17)$$

where we have made use of the fact that T_0 lies below the melting range and $\psi(T_m)$ is a normalized distribution, hence

$$\int_{T_0}^{T_m^0} \psi(T_m)\mathrm{d}T_m = 1 \quad (18)$$

Since equation (3) allows for the possibility of structural evolution, it can be applied here to predict recovery following setting by melting and recrystallization. Substituting from equations (17) into equation (3) yields the fractional recovery

$$f = \int_{T_s}^{T_m^0} \psi(T_m)\mathrm{d}T_m \quad (19)$$

The relation between f and $\psi(T_m)$ predicted is shown in the sketch of *Figure 3b*. Equation (19) can be inverted, of course, to yield the analogue of equation (9)

$$\psi(T_m) = -\left.\frac{\mathrm{d}f}{\mathrm{d}T_s}\right|_{T_s = T_m} \quad (20)$$

Now that the two hypotheses for heat-setting – viscous flow and melting/recrystallization – are both expressed in quantitative form, it will be possible to critically compare their predictions with experiment. It will be noted that there are clear parallels between them. Both attribute setting to stress relaxation at the setting temperature. The critical difference lies in *which parameter* triggers the stress relaxation and hence causes $G_e(t,0)$ to fall below $G_e(t-t_C,t_C)$ and a set to be achieved ($f<1$). For viscous flow, stress relaxation is *time-triggered*, f being determined solely by the equivalent time ζ_s allowed for setting (*Figure 3a*). For melting/recrystallization, stress relaxation is *temperature-triggered*, f being determined solely by the temperature T_s reached during setting (*Figure 3b*).

EXPERIMENTAL

Materials studied

The specimens studied were cut from oriented poly(ethylene terephthalate) monofilament, prepared at UMIST by melt-extrusion followed by drawing to a draw ratio of 5 at 80°C. Two monofilaments were used in the present work, one of 50 μm diameter, the other of 64 μm diameter. Both were prepared from the same batch of ICI fibre-grade PET, and were found to have indistinguishable physical properties. Density at 20°C was found to be 1381 kg m^{-3}, and birefringence was found to be 0.210. The number-average molecular weight ($\bar{M}_n$) was 2.0×10^4, as deduced from intrinsic viscosity (i.v.) measurement on the polymer in solution in *o*-chlorophenol, using the $\bar{M}_n$/i.v. relation obtained by Ravens and Ward[55]. The filaments were stored, in the dark, in a conditioned laboratory at 20°C, 65% relative humidity, for 3–4 years before being tested.

Heat-setting experiments

A schematic diagram of the main elements of the heat-setting experiment is given in *Figure 1*. In the present

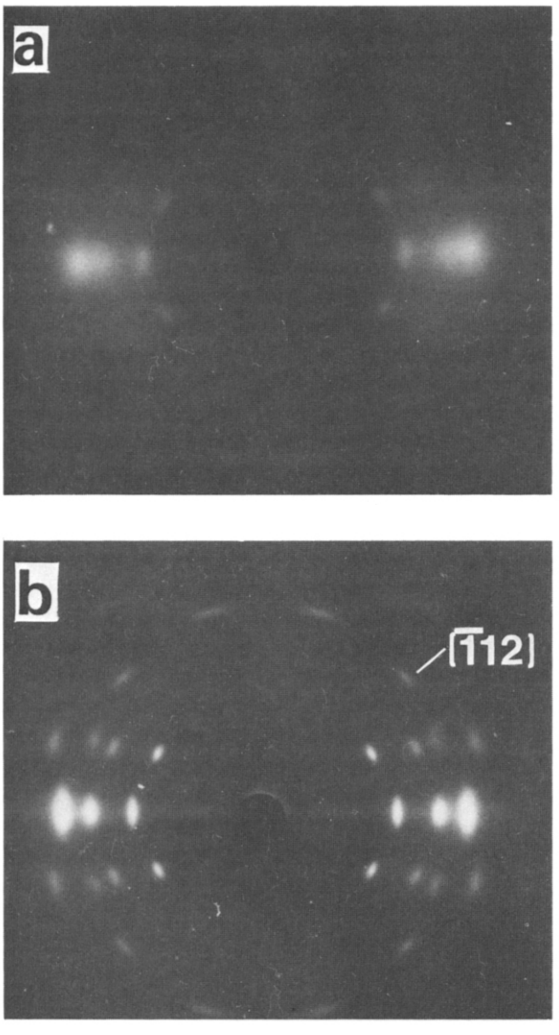

Figure 5 WAXS patterns obtained from drawn PET filaments: (a) as-drawn; (b) heat-set at 240°C for 120 s. Fibre axis is vertical

work the following conditions were kept constant: $T_0 = 20°C$, $t_A = 60$ s, $t_C - t_B = 60$ s, $t_D - t_C = 300$ s. In all experiments reported here, the mode of deformation was torsion of the filament about its own axis, and the maximum skin shear strain induced, γ_0, was kept at 0.006, unless otherwise stated; this was within the linear viscoelastic region for the filaments, to within experimental precision. Primary experimental variables were the time and temperature of heat-setting, t_s and T_s, and the thermal pre-treatment of the filaments.

In summary, the experimental sequence was as follows.

(1) *Removal of initial twist.* The 100 mm length of filament was freely suspended with a 1.3 g brass vane attached to its lower end, to allow slight twist remaining from the original winding of the filament on the bobbin to recover.

(2) *Insertion of twist.* The filament was clamped at constant length and twisted about its own axis at room temperature.

(3) *Heat.* The filament was gripped in a clamp at constant length and twist and immersed in thermostatically controlled silicone oil at the required setting temperature T_s for a time t_s. T_s was held constant to ± 0.1 K.

(4) *Cool.* The filament was removed from the oil and quenched in silicone oil at room temperature.

(5) *Release.* The filament was suspended in a draught-free box at room temperature, and released, allowing it to freely untwist.

(6) *Measurements.* The twist recovery was measured. The rotation of the brass vane was monitored to determine the twist recovery. Whole numbers of rotations were counted by using a photoelectric cell and electronic digital counter, and fractions of a rotation were read from the position of the brass vane using a concentric protractor. It was found that the final angular position of the vane could be resolved to $\pm 5°$. Fractional recovery f was taken to be the fraction of surface shear strain (tangent of surface shear angle), which was recovered on release of the filament.

A new filament specimen was used for each heat-setting measurement. Repeat measurements on 20 specimens tested under identical conditions gave a value for the standard deviation in measurements of fractional recovery of 0.004, for a skin shear strain $\gamma_0 = 0.006$.

Specimens thermally pre-treated before heat-setting in torsion were held at constant length and zero twist and immersed in thermostatically controlled silicone oil at the required pre-setting temperature T_p for a time t_p, before beginning the sequence described above.

To assist in the interpretation of heat-setting measurements, it was found helpful to know the room-temperature shear modulus of the material following thermal pre-treatment. This was measured by suspending a filament specimen as a torsional pendulum, with a calibrated miniature inertia bar attached to its lower end providing a known inertia. The real part of the dynamic shear modulus, G', was determined for a frequency of 0.060 Hz.

Microstructural measurements

Density was measured on small loops of the filament samples, with a density gradient column at 23°C. The column liquids used were carbon tetrachloride and n-heptane. Fifteen hours were allowed for equilibration of specimens in the column before readings were taken. Negligible drift in position was observed after this time. It was found that measurements could be resolved to 0.1 kg m^{-3}. Density values were used to give an indication of changes in degree of crystallinity, notwithstanding the known difficulty of obtaining consistent values of crystallinity for PET. An apparent volume fraction crystallinity χ_{vp} was estimated from density ρ, using values for the crystal density (ρ_c) and non-crystalline density (ρ_{nc}) of 1455 kg m^{-3} (ref. 56) and 1335 kg m^{-3} (ref. 57) respectively.

Wide-angle X-ray scattering (WAXS) and small angle X-ray scattering (SAXS) experiments were achieved with a single Laue X-ray camera and pin-hole collimated, nickel-filtered Cu Kα radiation. Intensities on photographic negatives were measured on a Joyce–Loebl scanning microdensitometer. Within each of the two sets of WAXS and SAXS photographs, conditions of X-ray exposure and photographic development were carefully kept constant, so that measured intensities could be compared.

WAXS patterns took the usual form for oriented fibres of PET. *Figure 5* shows patterns for the two extremes of

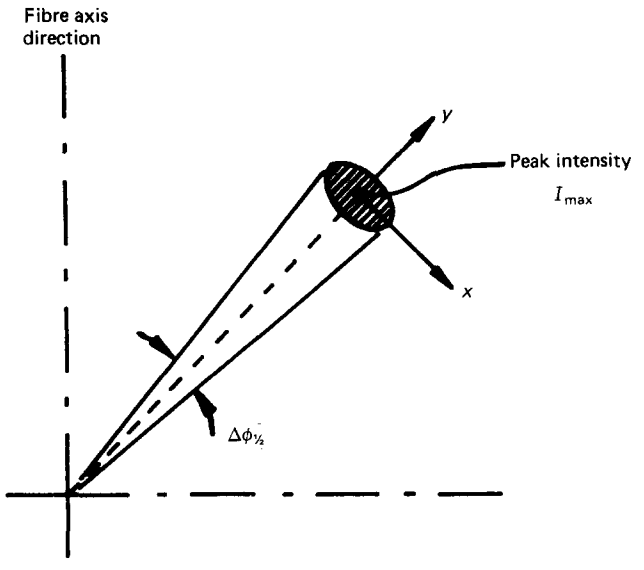

Figure 6 Schematic sketch of (1̄12) diffraction spot showing directions x and y of intensity measurement scans

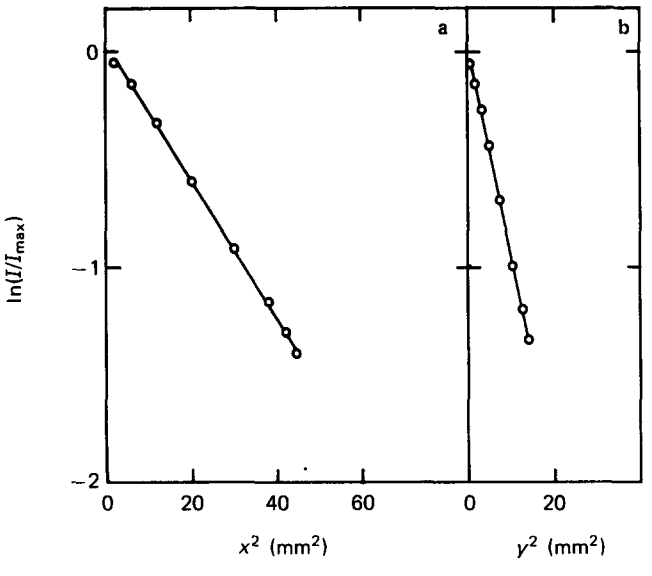

Figure 7 Typical semi-log plots of intensity *versus* x^2 or y^2 from scans of (1̄12) diffraction spots in (a) azimuthal and (b) radial directions. Full lines through data show agreement with equations (21)

(a) unannealed and (b) highly annealed (240°C for 2 min) specimens. In the present work, quantitative measurements were made only on the (1̄12) reflections. These were chosen because they were distinct and relatively isolated diffraction spots, only overlapping slightly the edge of the 'amorphous halo'. Intensity was scanned along azimuthal and radial directions, as shown schematically in *Figure 6* as directions x and y. In all cases, it was found that the intensity varied with position as a Gaussian function, to a good approximation. Thus

$$I = I_{max}\exp(-K_x x^2) \qquad I = I_{max}\exp(-K_y y^2) \quad (21)$$

for azimuthal and radial scans respectively. Typical examples are given in *Figure 7*. The measured values of peak intensity I_{max} and Gaussian decay factors K_x and K_y were used to obtain three morphological parameters.

(1) Relative crystallinity as determined by X-ray scattering. The integrated intensity I_{int} was obtained by integration of I given by equations (21), assuming the (1̄12) reflections to be elliptical in shape, hence

$$I_{int} = \frac{\pi I_{max}}{\sqrt{K_x K_y}} \quad (22)$$

It was expressed as a fraction of I_{int} for the most highly annealed specimen I_{int} (240°C/120 s).

(2) Degree of crystal orientation, as expressed by the half-width $\Delta\phi_{1/2}$ of the angular spread of crystal c axes about the fibre axis. This was obtained from K_x.

(3) Crystal size, as expressed by the crystal width W(1̄12) normal to (1̄12) planes. This was obtained from K_y via the approximate form of the Scherrer equation

$$W = \frac{\lambda}{\Delta(2\theta)_{1/2}\cos\theta} \quad (23)$$

where λ is the X-ray wavelength and $\Delta(2\theta)_{1/2}$ is the half-width (in radians) of the angular spread of the diffraction spots in the radial direction.

SAXS patterns were found to be of the 'two-point' type, showing elongated 'spots' on meridional layer lines of first order, elongated perpendicular to the fibre axis (an example is given in *Figure 8a*). *Figure 8b* is a schematic diagram of the pattern, indicating the parameters measured by microdensitometer scans along x and y directions defined as shown. It is not possible to derive precise structural details from such limited information on such a diffuse scattering pattern. The problems involved in interpretation were recently reviewed by Hall

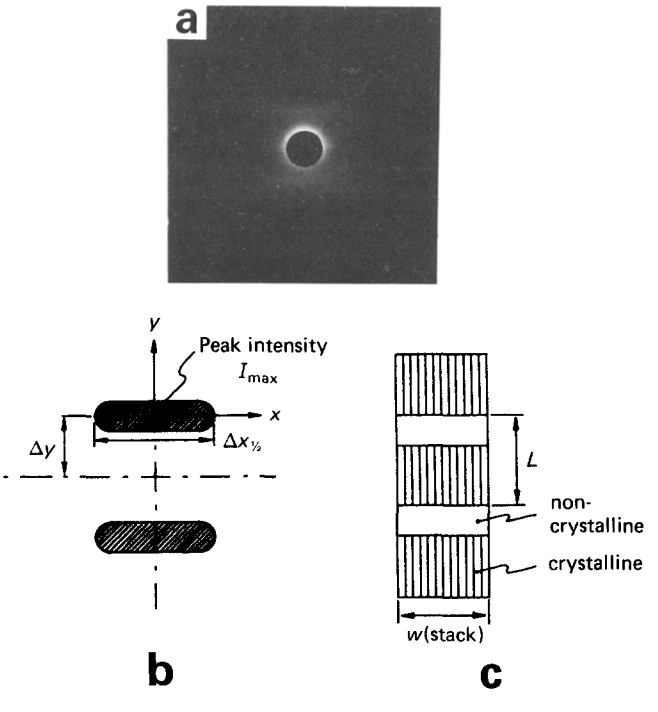

Figure 8 SAXS patterns from drawn PET filaments: (a) pattern obtained after heat-setting at 240°C for 120 s; (b) schematic diagram of pattern in (a); (c) idealized structural model used in interpreting SAXS patterns. Fibre axis is vertical

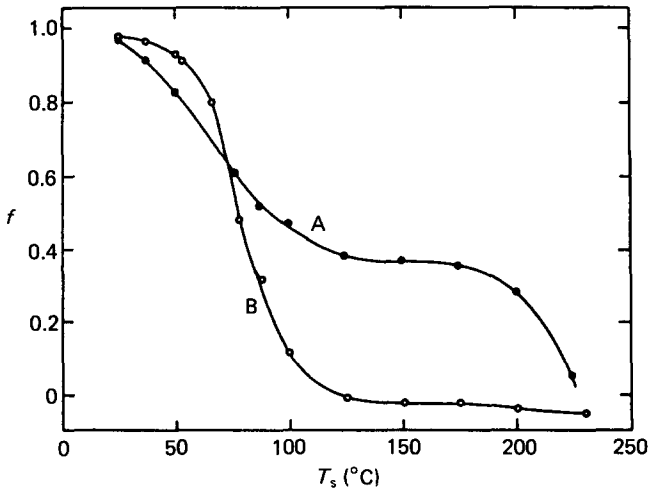

Figure 9 Fractional recovery, f, *versus* setting temperature, T_s, for (A) pre-set, and (B) not pre-set, filaments of drawn PET heat-set in torsion at constant length for a time $t_s = 120$ s

and Toy[58]. For purposes of comparison of specimens in the present work, however, the data were treated as if arising from identical fibrillar stacks of regularly alternating crystalline/non-crystalline units as sketched in *Figure 8c*. In terms of this idealized structural model, two morphological parameters were derived: (1) the repeat distance of the linear lattice, or 'long period', L, which was found from the layer line spacing Δy, by simple application of Bragg's Law; (2) the width of the fibrillar stack, W(stack), which was found from the half width of the spots $\Delta\chi_{1/2}$, as measured along the layer line, by applying the Scherrer equation (23).

In addition, the relative peak intensity was recorded: I_{max} expressed as a fraction of I_{max} for the most highly annealed specimen I_{max} (240°C/120 s). I_{max} is proportional to $(\rho_c - \rho_{nc})^2$ if other structural features remain constant.

In presenting measurements obtained from X-ray scattering patterns, we have used bars to indicate uncertainty in the measurements resulting from random scatter. Further experimental details have been given elsewhere[59].

Calorimetry

Melting of the PET filaments was studied by calorimetry, at a constant heating rate of 20 K min^{-1}. The instrument used was a Perkin Elmer DSC2 Differential Scanning Calorimeter. Specimens were prepared by tying 10 filaments into loops small enough to fit in the specimen capsule. In this way specimen masses were achieved in the range 0.39–0.67 mg.

HEAT-SETTING RESULTS

Figure 9 shows the change in fractional recovery, f, with setting temperature, T_s. For specimens pre-set at $T_p = 200$°C, $t_p = 2.1 \times 10^3$ s (curve A) the decrease in f occurs in two distinct steps. The low-temperature process is centred at about 75°C and is clearly the glass transition in PET. There is then a plateau region followed by a second, high-temperature process, which begins at about 175°C and is centred at about 205°C. It is noteworthy that the high-temperature process begins at a value of T_s that is 25 K below T_p and that zero recovery is obtained some 30 K below the apparent melting point of PET (*ca.* 250°C, see below).

For fibres that have not been pre-set (*Figure 9*, curve B), complete set is achieved in the region of the glass transition and the second process is not evident. Another noteworthy point in *Figure 9* is that for the untreated specimens, values of f become slightly negative at $T_s > 125$°C. This effect, known as 'overtwist', is caused by a small contribution from the anisotropy of thermal expansion and has been discussed in detail elsewhere[45].

Heat-setting in the glass-transition region is to be expected, in view of the stress relaxation occuring here (see the earlier section on heat-setting by viscoelasticity). The main interest in *Figure 9* lies in the high-temperature process, visible in pre-treated specimens only. In such specimens, this is the mechanism by which f falls to zero and a complete set is achieved. Experiments were made, therefore, to gain further information on the nature of the high-temperature process. For the same pre-setting conditions as apply in *Figure 9*, $T_p = 200$°C, $t_p = 2100$ s, recovery from heat-set was measured for varying setting times t_s, at several temperatures T_s in the region of the high-temperature process. Results are given in *Figure 10* with T_s as parameter (full lines).

The dominant feature to emerge is the pronounced dependence of f on heat-setting time t_s, as well as on temperature T_s. The effect of changing T_s is clearly to accelerate or decelerate the time-dependent decay of f, causing a shift of the centre of the process along the logarithmic timescale.

Following discovery of this well defined high-temperature process, further experiments were made to investigate its dependence on the structural state of the material. Specimens were prepared with thermal pre-treatments (at constant length and zero twist) for various combinations of temperature T_p and time t_p. Microstructural measurements were also made on heat-set specimens: results are presented in the next section.

The dominant effect of varying T_p at constant t_p can be seen in *Figure 11* for $t_p = 2100$ s. The temperature position of the process clearly shifts upwards with increasing T_p; at the same time, the plateau in f separating the process from

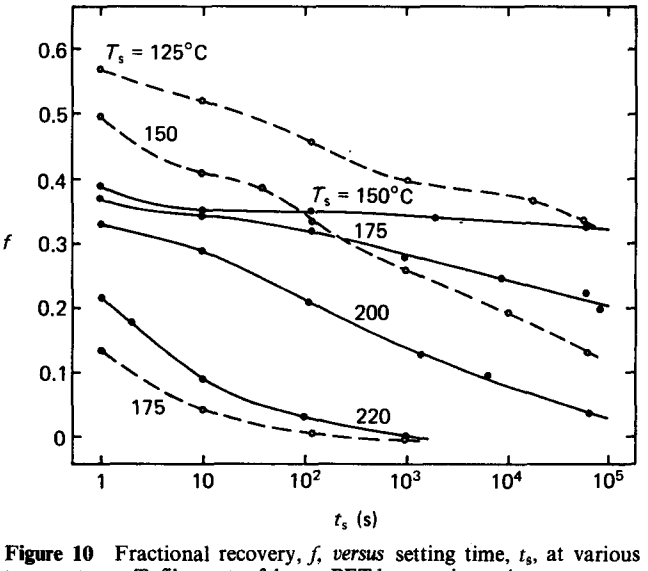

Figure 10 Fractional recovery, f, *versus* setting time, t_s, at various temperatures, T_s: filaments of drawn PET heat-set in torsion at constant length after pre-setting at $T_p = 200$°C, $t_p = 2100$ s (full lines) or $T_p = 150$°C, $t_p = 2100$ s (broken lines)

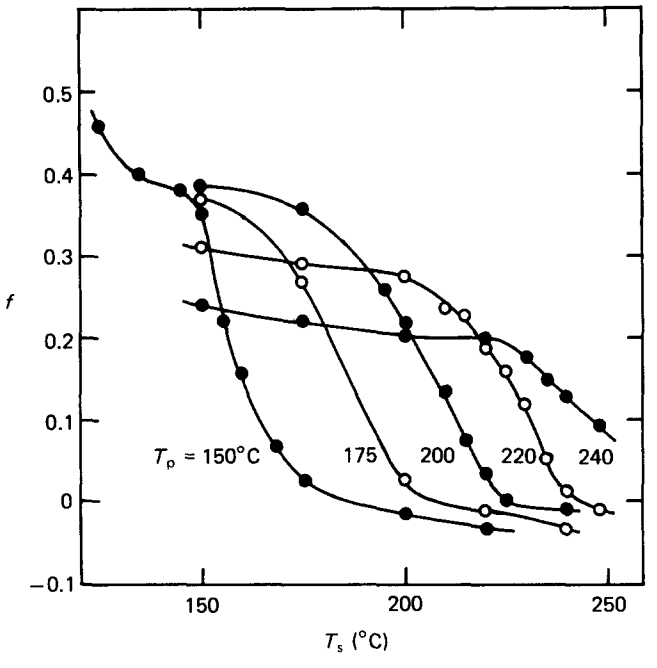

Figure 11 Effects of varying pre-setting temperature, T_p, on the fractional recovery, f, following heat-setting at temperatures T_s and time $t_s = 1.20$ s ($t_p = 2100$ s)

the glass transition falls with increasing T_p. The mechanism by which the pre-treatment shifts the high-temperaure process appears to be by changing the time constant for decay of f. This can be seen in *Figure 10*, where the time dependence of f for $T_p = 200$°C (full lines) is compared with that for $T_p = 150$°C (broken lines). Comparing results obtained at a given T_s, it appears that raising T_p from 150 to 200°C has shifted the decay of f to very much longer times (by a factor of more than 10^5 (see the curves for $T_s = 175$°C)).

The effect of varying pre-setting time t_p at constant T_p is shown in *Figure 12* for $T_p = 200$°C (similar results were obtained at 220°C and 240°C). Two effects appear to be general. With increasing t_p there is a shift of the high-temperature process to higher setting temperatures T_s. In this respect the effects of increasing t_p and T_p appear to be similar. The plateau in f, however, behaves differently. With increasing t_p it increases (*Figure 12*), whereas with increasing T_p it decreases (*Figure 11*). The combined effect of these two trends with increasing t_p is to cause the high-temperature process to be only a relatively indistinct shoulder on the side of the glass transition for short pre-setting times t_p (e.g. 1 s), but to evolve into a well delineated separate process at longer times t_p.

MICROSTRUCTURAL VARIATIONS

To assist interpretation of the recovery measurements, a study was made of microstructural variations taking place during heat-setting. Specimens were prepared as for the twist recovery tests, but without the insertion of twist.

Density and crystallinity

There is a well known problem with PET in obtaining meaningful measurements of degree of crystallinity. The reason is that the properties of crystal and amorphous fractions are not fixed, but vary somewhat, depending on the thermal history of the material[17,19,26]. In this situation, to make reliable deductions about crystallinity changes, it is necessary to seek corroboration between different methods of measurement. In the present work this was done by comparing density measurements with WAXS intensity measurements.

In *Figure 13* is shown the variation of density with heat-setting temperature T_s for (A) specimens without a pre-setting sequence, and (B) specimens pre-set at 200°C for 2100 s. On the right side of *Figure 13* is given the corresponding scale of apparent volume fraction crystallinity, as determined from density, χ_{vp}. The other measure of crystallinity obtained – the relative crystallinity as determined from WAXS intensity – is shown in *Figure 14* for specimens heat-set at different temperatures T_s. There is a clear parallel between the curves shown in *Figures 13* (curve A) and *14*. The degree of crystallinity shows an initial slight fall to values of T_s in the glass transition region, and then a steady increase with increasing T_s up to the melting region. For specimens pre-set at 200°C (*Figure 13*, curve B) density (and presumably crystallinity) does not change during setting until the setting temperature T_s exceeds 200°C.

The changes in density (and χ_{vp}) with time t_s are plotted in *Figure 15* with T_s as parameter. It can be seen that for $T_s \geqslant 150$°C there is a rapid increase in density from the initial value of 1381 kg m^{-3}, followed by a slow but steady increase with increasing time t_s.

The fact that properties of crystalline and non-crystalline fractions change during heat-treatment is emphasized by the measurements of SAXS intensity presented in *Figure 16*, where a large increase is apparent with increasing T_s. The effect is widely observed during heat treatment of semicrystalline polymers, and has been reported previously for heat-treated drawn PET[10,19]. For degrees of crystallinity around 50%, and for unchanged crystal surface orientation, SAXS intensity is proportional to $(\rho_c - \rho_{nc})^2$, as mentioned earlier. So *Figure 16* suggests an increase in $\rho_c - \rho_{nc}$ by a factor of 2 between $T_s = 175$°C and 240°C. This is most probably due

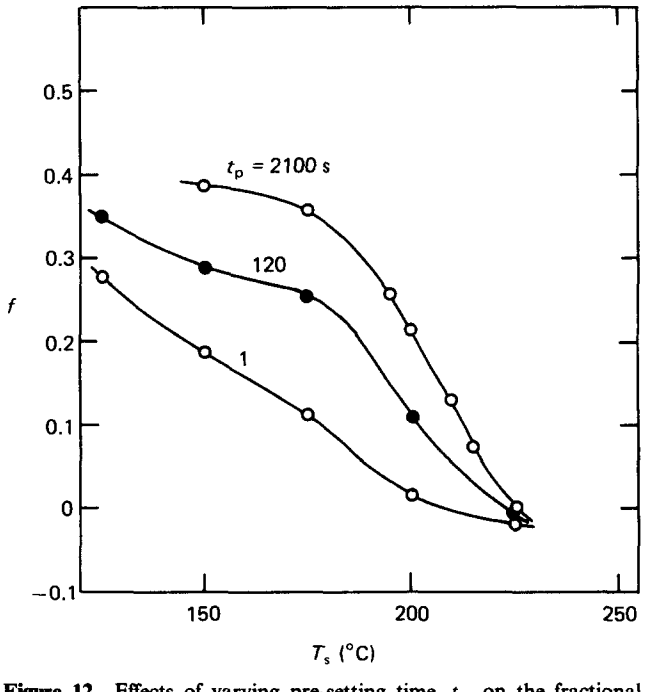

Figure 12 Effects of varying pre-setting time, t_p, on the fractional recovery, f, following heat-setting at temperature T_s and time $t_s = 120$ s ($T_p = 200$°C)

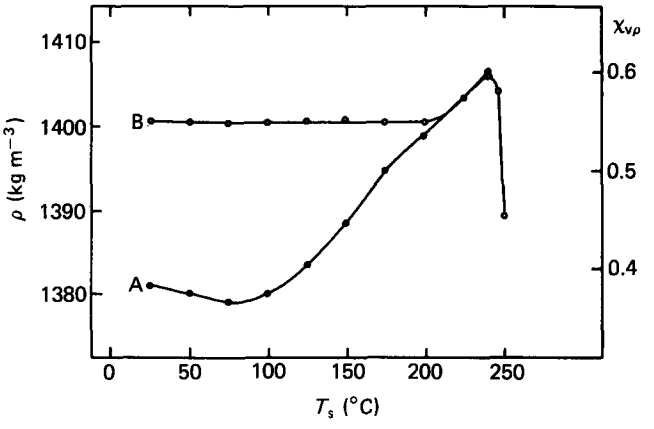

Figure 13 Density, ρ, and apparent volume fraction crystallinity, $\chi_{v\rho}$, following heat-setting at temperature T_s and time $t_s = 120$ s: (A) not pre-set; (B) pre-set at $T_p = 200$°C and $t_p = 2100$ s

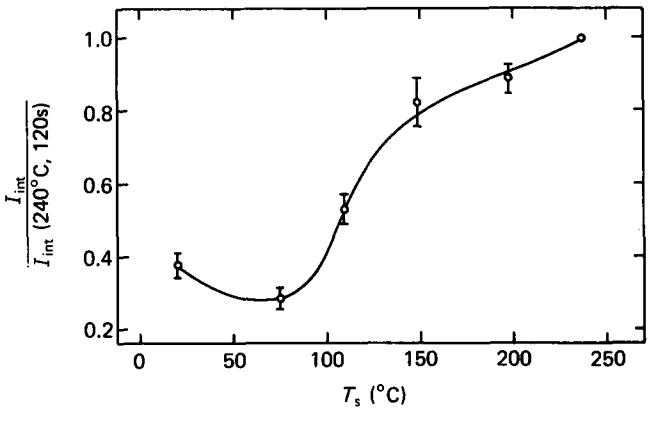

Figure 14 Relative WAXS integrated intensity for the ($\bar{1}12$) reflection following heat-setting at temperature T_s and time $t_s = 120$ s

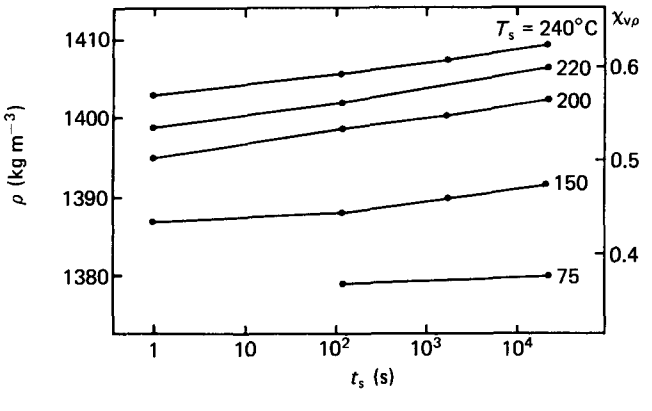

Figure 15 Density, ρ, and apparent volume-fraction crystallinity, $\chi_{v\rho}$, following heat-setting at various times t_s and temperatures T_s

to both an increase in crystal perfection (increase in ρ_c) and increasing randomization of the non-crystalline fraction (decrease in ρ_{nc}). As *Figure 16* also shows, SAXS intensity was found to increase with increasing time t_s at constant T_s.

Crystal size and orientation

A measure of crystal size is given by $W(\bar{1}12)$ determined from the radial spread of the ($\bar{1}12$) diffraction spots. This quantity is shown in *Figure 17*, plotted *versus* setting temperature T_s. The method of calculation of $W(\bar{1}12)$ from the Scherrer equation (see Experimental section) is such that it gives a *lower* limit to the crystal extent normal to ($\bar{1}12$); it ignores lattice disorder within the crystals, which would also contribute to broadening of diffraction spots (as would the finite X-ray beam width). Thus the increase in $W(\bar{1}12)$ with increasing T_s shown in *Figure 17* can be interpreted as an increase in crystal size and/or a decrease in lattice disorder.

Other measures of crystal size are available, however, from SAXS patterns, so the width of crystals perpendicular to the fibre axis is indicated by W(stack); this is shown plotted *versus* T_s in *Figure 18*. Again there is a tendency for W(stack) to increase with increasing T_s, especially at the highest temperatures. W(stack) also increases with increasing time t_s at constant T_s (see *Figure 18*). Crystal size parallel to the fibre axis is indicated by the long period L, shown plotted *versus* T_s in *Figure 19*. Again, L increases with increasing T_s, consistent with previous observations[5,7,8,10,15,19]. There are also small increases with increasing t_s at constant T_s.

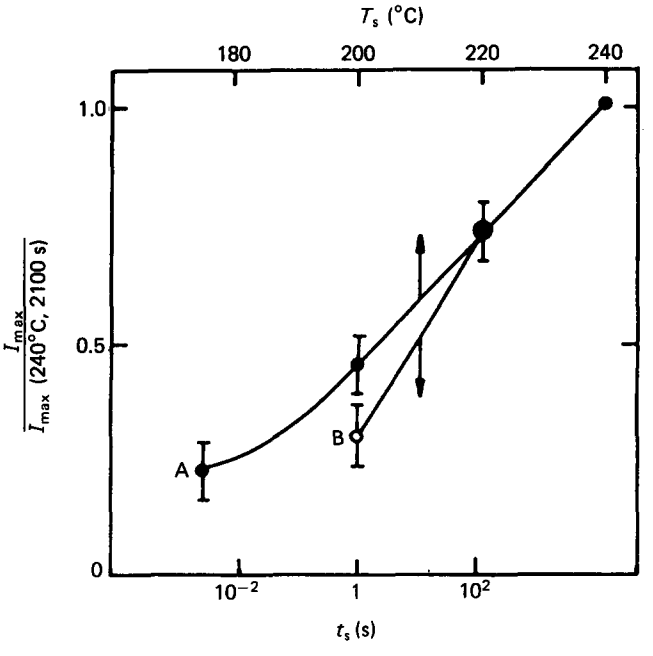

Figure 16 Relative SAXS maximum intensity following heat-setting: (A) *versus* T_s at constant $t_s = 120$ s; (B) *versus* t_s at constant $T_s = 220$°C

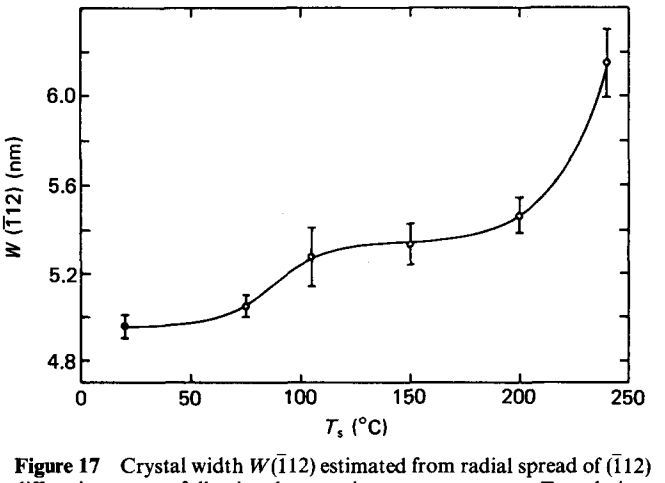

Figure 17 Crystal width $W(\bar{1}12)$ estimated from radial spread of ($\bar{1}12$) diffraction spots, following heat-setting at temperature T_s and time $t_s = 120$ s (open symbols), and unset (filled symbol)

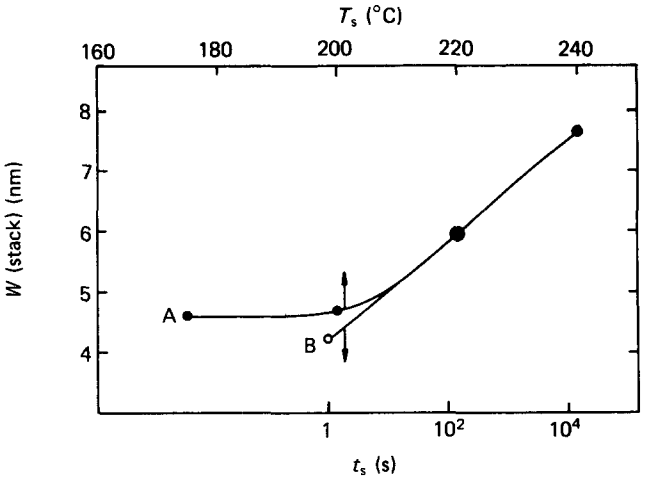

Figure 18 Width, W(stack), of fibrillar stacks of crystals, estimated from lateral spread of first-order layer lines in SAXS patterns following heat-setting: (A) *versus* T_s at constant $t_s = 120$ s; (B) *versus* t_s at constant $T_s = 220$°C

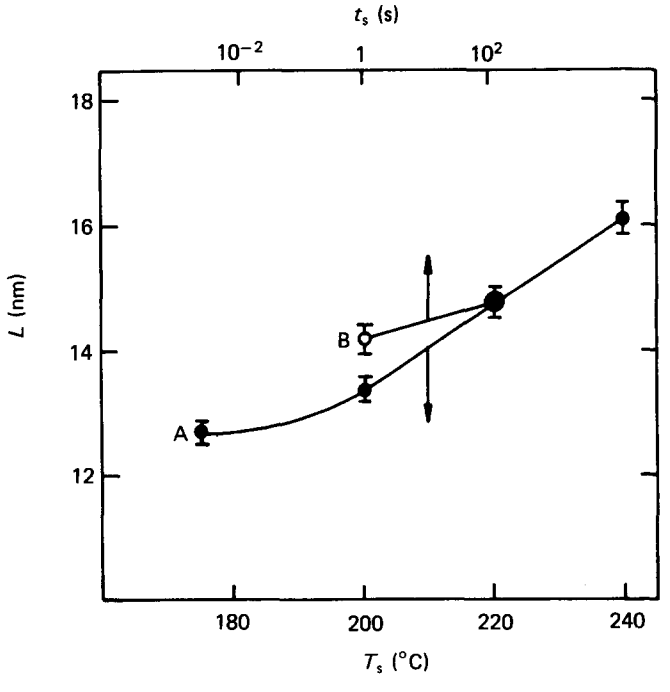

Figure 19 Long period, L, of fibrillar stacks of crystals, estimated from separation of first-order layer lines in SAXS patterns following heat-setting: (A) *versus* T_s at constant $t_s = 120$ s; (B) *versus* t_s at constant $T_s = 220$°C

The degree of crystal orientation was observed from the azimuthal spread of ($\bar{1}12$) diffraction spots. The half-width of the angular distribution $\Delta\phi_{1/2}$ is shown in *Figure 20* plotted *versus* T_s. It is apparent that crystal orientation increases with increasing T_s. This has been shown before for drawn PET heat-treated at constant length[39].

INTERPRETATION OF RESULTS

Mechanism of heat-setting

The two most likely origins of the high-temperature heat-setting process are viscous flow and melting/recrystallization. Before examining these, however, it is necessary to eliminate alternatives.

A possibility that cannot be discounted is that the process is associated with yield, as in the forming of metals. If this were the case it would occur only when the strain exceeded a critical yield strain. Experiments were conducted to test this possibility for the drawn PET studied here. Heat-setting experiments were made on specimens pre-set at $T_p = 200$°C, $t_p = 2100$ s, by using the procedure outlined in the Experimental section, but with various skin shear strains γ_0. The recovered skin shear strain γ_r was determined as a function of γ_0. *Figure 21* shows results obtained at $T_s = 150$°C and 200°C. These two setting temperatures were chosen for being in the temperature regions of the plateau and of the high-temperature process, respectively, for specimens pre-set at 200°C/2100 s. For comparison, the broken line in *Figure 21* shows what would be obtained if $f = 1$ (no set). It is clear from this figure that the curves obtained at $T_s = 150$°C and 200°C are quite distinct: they do not coincide even in the very low strain linear region. Thus the reduction in f from $T_s = 150$°C to 200°C appears to persist to vanishingly small strains, ruling out the possibility that the high-temperature process is associated with yield.

A further possibility that needs consideration is that the stress relaxation at T_s causing the high-temperature process is the result of hydrolytic attack on the PET molecules, caused by the combination of high temperature and absorbed moisture. Such a mechanism is always a possibility in condensation polymers such as PET during heat-setting; it was tested as follows. Two families of specimens were prepared by pre-treating at 200°C/2100 s. One family was heat-set as described in the

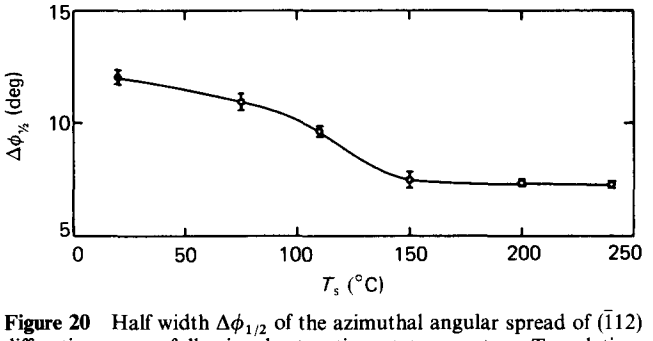

Figure 20 Half width $\Delta\phi_{1/2}$ of the azimuthal angular spread of ($\bar{1}12$) diffraction spots, following heat-setting at temperature T_s and time $t_s = 120$ s (open symbols), and unset (filled symbol)

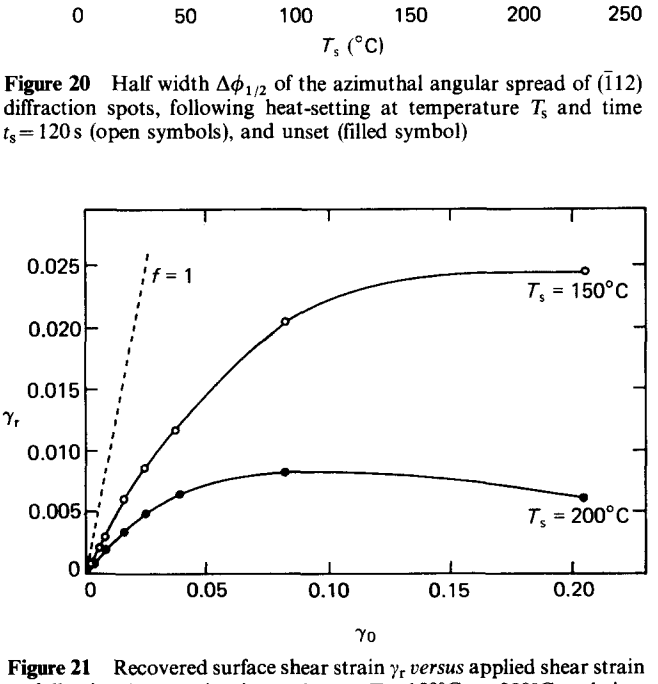

Figure 21 Recovered surface shear strain γ_r *versus* applied shear strain γ_0 following heat-setting in torsion at $T_s = 150$°C or 200°C and time $t_s = 120$ s. Pre-setting conditions: $T_s = 220$°C, $t_s = 2100$ s. Broken line represents full recovery

Table 1 Effect of pre-drying on the fractional recovery of PET filaments following heat-setting for $t_s = 120$ s at various temperatures T_s (specimens were previously heat-treated at constant length at 200°C/2100 s)

	f	
T_s (°C)	Dried	Undried
125	0.388	0.384
150	0.375	0.370
175	0.353	0.358
200	0.281	0.285
225	0.049	0.053

Experimental section for $t_s = 120$ s at various temperatures T_s. The other family were heat-set similarly, except for the one difference that these specimens were dried in a dessicator under vacuum at room temperature for 1 h, after being twisted. After drying, they were immediately heat-set in silicone oil by the usual method. Results are given in *Table 1*. It is clear that, to within the random measuring error in f of 0.004, the two sets of results are indistinguishable. This is convincing evidence that hydrolysis is not the origin of heat-setting.

The dominant hypothesis for the mechanism of high-temperature heat-setting in semicrystalline polymers is that of melting/recrystallization. The behaviour to be expected according to this hypothesis was analysed in an earlier section. In particular, equation (20) relates the curve of f *versus* T_s to the distribution of melting points $\psi(T_m)$. For example, the inflection in f *versus* T_s should occur at the temperature of the peak in the function ψ (see *Figure 3b*). To test this hypothesis, therefore, calorimetric measurements of melting were made to find the distribution of melting points as revealed by specific heat C_p.

Example d.s.c. thermograms are shown in *Figure 22*, for specimens pre-set at various temperatures T_p, for $t_p = 120$ s. To test the hypothesis, compare the curves in *Figure 22* with the heat-setting results in *Figure 11*. It will be seen that, whereas the high-temperature inflection in f shifts upwards in temperature with increasing T_p, and is usually not far removed from T_p, the melting peaks in C_p in *Figure 22* are virtually stationary on the temperature scale as T_p is increased. Two melting peaks are visible, the first occurring at 247°C, the second at 253°C. Except for $T_p = 240$°C, no peak in C_p was detectable in the temperature regions of the inflections in f *versus* T_s. This discrepancy between the curves of f *versus* T_s and the melting peaks in C_p appears to provide strong evidence against the melting/recrystallization hypothesis. On close examination, however, the evidence is not so conclusive. The double melting peaks shown in *Figure 22*, and widely reported elsewhere for PET, are now generally believed to be the net result of a continuous process of melting and recrystallization during heating in the d.s.c.[60–64]. So, the second melting peak probably corresponds to melting of crystals formed from the melt provided by the first melting peak. This was demonstrated in the present work by the fact that no separate second peak was observed at high d.s.c. heating rates (e.g. 80 K min^{-1})[59], because of insufficient time being available for recrystallization. Moreover, Berndt and Bossman[65] and Weigmann *et al.*[66] *did* find a small peak in C_p in the temperature region of a previous heat-treatment when studying drawn PET (such peaks have also been widely reported in undrawn PET). They used differential thermal analysis (d.t.a.) and d.s.c., respectively, at very high sensitivity. These peaks were extremely small in magnitude compared to the final melting peaks; attempts to find them in the present work failed. Nevertheless, the fact that they have been observed in specimens prepared in a similar manner to those studied here, and the fact that they apparently increase in magnitude with increasing heating-rate[65], mean that the melting curves of *Figure 22* may be misleading. It is possible that the first melting peak simply represents the melting of crystals whose melting point has been raised by annealing during heating in the d.s.c.: the point is not proven. There is sufficient doubt, however, for the curves of *Figure 22* not to be regarded as reliable indicators of the melting behaviour of the crystals existing before the d.s.c. experiment. Therefore d.s.c. does not provide an unambiguous test of the melting/recrystallization hypothesis, which might be assumed.

There are, however, other results among those presented here which cast doubt on melting/recrystallization and favour the viscous flow hypothesis. Consider the heat-setting results given in *Figures 9–12*. It will be seen that the high-temperature process begins at temperatures T_s below T_p. According to the melting/recrystallization hypothesis, however, $-df/dT_s$ gives $\psi(T_m)$ at $T_m = T_s$ (equation (20)); therefore a finite gradient in $f(T_s)$ at $T_s < T_p$ means that the distribution $\psi(T_m)$ extends to below T_p, so there are crystals present that melt at a temperature below that where they were formed (assuming they were formed at T_p and not during cooling from T_p). This possibility can be rejected. Thus the melting/recrystallization does not provide a consistent explanation for the results.

Perhaps the major evidence in favour of the viscous-flow hypothesis is the pronounced time-dependence of heat-setting in the high-temperature region, as shown in *Figure 10*. If heat-setting occurred by melting/recrystallization, it would be *temperature-triggered*. Time would only be needed for heat transfer through the filaments ($\ll 1$ s for filaments less than 100 μm in diameter in silicone oil). By contrast, the steady decay of f with

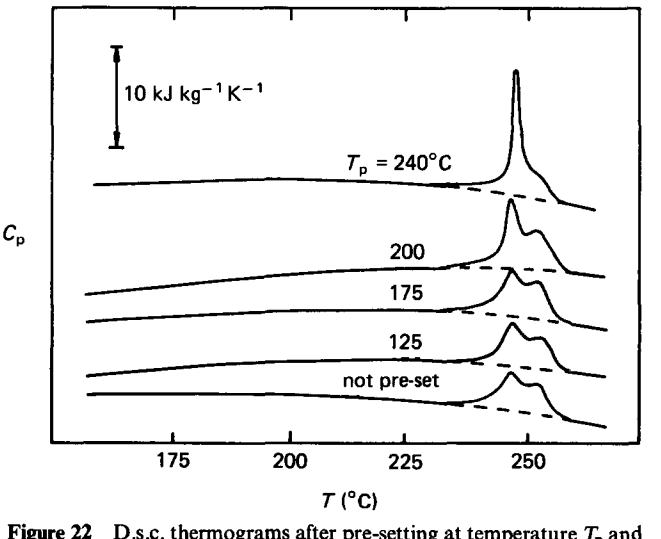

Figure 22 D.s.c. thermograms after pre-setting at temperature T_p and time $t_p = 120$ s (heating rate 20 K min^{-1}). Successive curves have been displaced vertically to avoid overlap

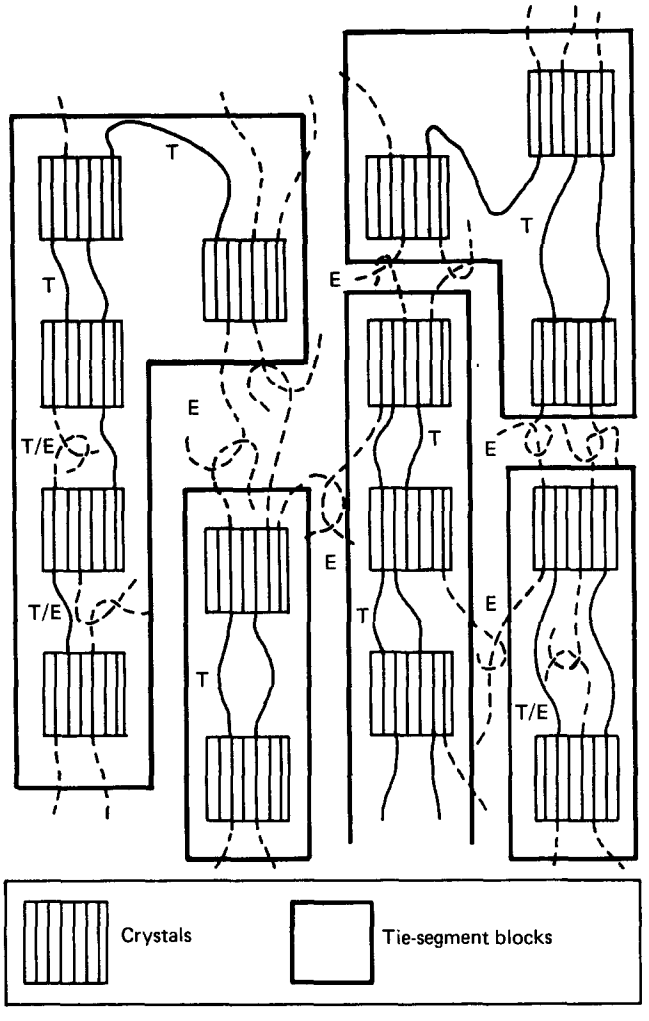

Figure 23 Schematic structural model for drawn PET, illustrating the three possible modes of intercrystalline molecular connection: tie-segments only (T); entanglements only (E); tie-segments plus entanglements (T/E). A group of crystals interconnected by tie-segments constitutes a 'tie-segment block'

increasing t_s, followed here for periods of up to 24 h, and the temperature-induced acceleration and deceleration of this decay are characteristic of the recovery behaviour of a viscoelastic fluid. In conclusion the weight of evidence is in favour of the high-temperature process corresponding to viscous flow.

The small 'melting' peaks in d.t.a. and d.s.c. observed near pre-setting temperatures by others are not necessarily inconsistent with this conclusion. First, they may not be 'melting' peaks at all in the true sense, meaning dissolution of crystals in the melt. It is now well known that peaks in C_p can be obtained even in non-crystalline polymers, following heat-treatment in the region of a mechanical relaxation process, for example the glass transition[67]. They may purely reflect the time-dependent response of the specimen's enthalpy to the constant heating-rate imposed in the d.t.a. or d.s.c. test. Secondly, we do not need to rule out the possibility that partial melting occurs on re-heating to the region of the pre-setting temperature. It is simply that it does not appear to make a significant contribution to the set achieved.

If the high-temperature heat-setting process occurs by a viscous flow mechanism, as we suggest, it can be viewed as a purely mechanical relaxation independent of microstructural changes also taking place. It might, therefore, be termed the 'α'-relaxation' of PET, to distinguish it from the α-relaxation (glass transition) and β-relaxation occurring at lower temperatures. But to what molecular motion does it correspond?

At this stage any answer must be speculative. However, our suggestion is as follows. The molecular motion involved in the α'-relaxation is the slipping of entanglements by 'reptation', in the manner of a non-crystalline polymer in the 'terminal' zone beyond its rubber-like plateau. This behaviour is well known and has been reviewed amply elsewhere (see, for example, Ferry[68]). Such a mechanism is normally assumed not to apply to semicrystalline polymers below the melting region, as the crystals are presumed to provide a 'cross-linked' network capable of resisting flow. For PET, however, the low molecular weight of commercial samples (e.g. $M_n \approx 20\,000$–$30\,000$) combined with the poorly developed crystallinity, except in highly annealed specimens, make this relaxation mechanism likely. In detail, the process would differ from a non-crystalline polymer. A schematic diagram is given in *Figure 23*. Each crystal can be linked to any other crystal by direct molecular links (tie-segments) (T), indirect molecular links (via entanglements) (E) or combinations of both (T/E). Thus the complete structure consists of blocks of crystals interconnected by tie-segments, linked to other blocks by entanglements only. At temperatures above the glass transition, each tie-segment block behaves as a microscopic rubbery domain, with non-zero relaxed modulus. Total stress decay under constant strain, as occurs in the α'-relaxation, occurs by entanglement slippage *between* tie-segment blocks.

Another possibility is that the α'-relaxation occurs by axial and/or rotary molecular motion within the PET crystal, as is believed to be the case for the above T_g relaxations of other semicrystalline polymers (e.g. polyethylene, polypropylene, polyoxymethylene)[69]. Our data cannot rule this out. However, if it is so, the degree of sensitivity of the time/temperature position of the relaxation to thermal pre-treatment is unprecedented for a polymer crystal relaxation.

Time/temperature position of α'-relaxation

Equations (8)–(10) give the relations between heat-setting measurements and the relaxation spectrum ϕ. In particular, it may be seen from equation (10a) that for heat-setting at constant t_s, an inflection in f *versus* T_s gives the temperature where a maximum in ϕ occurs at $\tau = t_s$.

In the high-temperature region, the inflection was found to show a pronounced shift with increasing pre-setting temperature T_p (*Figure 11*). *Figure 24* shows plotted *versus* T_p the half height temperature $T_{1/2}$ (value of T_s where f is half the plateau value, this being better defined experimentally than the position of the inflection). It can be seen that there is almost a 1:1 relation between them. As heat-treatment proceeds during pre-setting, the structure evolves so as to bring the centre of the relaxation spectrum to a temperature/time position close to the prevailing pre-setting conditions. The significance of this observation appears to be that the evolution of microstructure is dependent on the same molecular diffusion processes as stress relaxation.

So, the overall picture is of a poorly crystallized, relatively low molecular weight polymer in which the

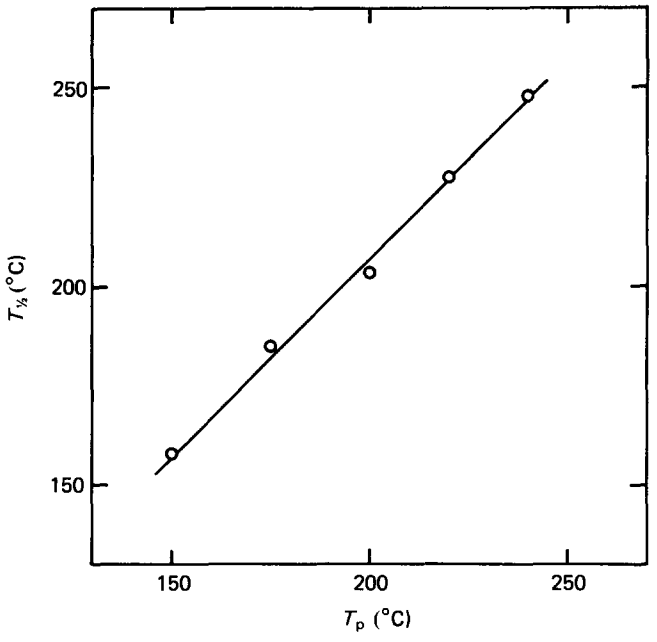

Figure 24 Temperature position of the centre of the α′-relaxation, $T_{1/2}$, as determined by heat-setting with $t_s = 120$ s, estimated from the data in *Figure 11*, showing dependence on pre-setting temperature, T_p, for constant $t_p = 2100$ s

crystals provide incomplete cross-linking, allowing entanglement slippage to give complete stress relaxation. On heat treatment, crystallinity develops further, providing more effective cross-linking and increasing the relaxation time for entanglement slippage, rather in the manner of a thermoset polymer approaching the gel point. The process of crystallization itself, however, requires molecular diffusion, and therefore can proceed at any given temperature only to the point where the dominant relaxation time *at that temperature* has reached the time allowed for crystallization.

This picture of events appears to account well for many of the observations here and elsewhere of the kinetics of microstructural evolution in drawn PET, as well as the relation of these to heat-setting measurements.

Magnitude of the α′-relaxation

The magnitude of the α′-relaxation is represented by the extent of modulus relaxation that occurs there. Since the relaxed shear modulus is zero for this relaxation, the relaxation magnitude is simply the modulus, G_i, in the intermediate, or plateau, region of the temperature scale that separates the α′-process from the α-process (glass transition). From equation (3), applied to the heat-setting conditions used in this work, G_i is related to the recovery f_i measured in the plateau temperature region by

$$f_i = G_i/G_e(300\text{ s}, t_C) \qquad (24)$$

Because of the fineness of the filaments used in the present work, it was not possible to measure the room-temperature shear stress relaxation modulus directly. However, it was estimated as the real part, G', of the dynamic shear modulus at low frequency (0.06 Hz), determined by torsion pendulum. Results are plotted in *Figure 25*, for specimens heat-treated at various temperatures T_p. It will be seen that, to within experimental scatter, G' (0.06 Hz) is independent of T_p, with a value of *ca.* 750 MN m^{-2}.

Since the room-temperature shear modulus shows no significant change with heat-treatment, the effects of heat-treatment on G_i can be deduced directly from its effects on recovery f_i (via equation (24)). How can the observed changes in magnitude of the α′-relaxation be understood in terms of the microstructural evolution that takes place during heat-treatment? This can be answered by means of a simple mechanical model of the polymer. The microstructure resembles a two-phase composite material, consisting of crystalline blocks dispersed in a non-crystalline matrix. The latter will act as a cross-linked rubber in the plateau region of temperature. Crystals stiffen the composite by (a) acting as rigid filler particles, and (b) partially cross-linking the rubbery matrix.

The mechanism of (a) is well known. The mechanism of (b), although widely invoked in an imprecise sense in the literature, needs to be expressed in precise quantitative terms consistent with current knowledge of microstructure before it can be used convincingly in the interpretation of results. This can be done by calculating the number of intercrystalline tie-segments per unit volume of the non-crystalline fraction, v. In addition, of course, there will be transient 'tie-segments', due to entanglements, active in the plateau region.

In the Appendix, the following expression is derived

$$v = \frac{1}{(1-\chi_v)}\left[\frac{1}{LA_0(\bar{n}+1)} - \frac{\rho N_0}{\bar{M}_n}\right] \qquad (25)$$

where A_0 is the cross-sectional area of the PET unit cell perpendicular to c, $\bar{n}$ is the mean number of chain-folds per molecule per crystal and N_0 is Avogadro's number. Consider a PET filament heat-treated at $T_p = 200$°C. The corresponding parameters needed in equation (25) can be estimated as follows: $\chi_v \simeq \chi_{v\rho} = 0.538$, $L = 13.4$ nm, $A_0 = 0.204$ nm^2, $\rho = 1400$ kg m^{-3}, $\bar{M}_n = 20000$, but $\bar{n}$ is unknown. Substituting yields

$$v \simeq (7.9/(\bar{n}+1) - 0.9) \times 10^{26} \text{ tie segments per cubic metre}$$

This can be visualized more readily, perhaps, in terms of the number-average tie-segment molecular weight $\bar{M}_t = N_0\rho/v$ that it implies,

$$\bar{M}_t = \frac{1067(\bar{n}+1)}{1-0.12(\bar{n}+1)}$$

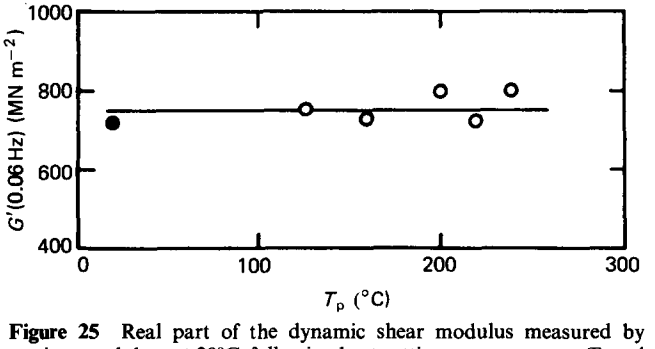

Figure 25 Real part of the dynamic shear modulus measured by torsion pendulum at 20°C, following heat-setting at temperature T_p and time $t_p = 120$ s (open symbols), and unset (filled symbol)

Recalling that the molecular weight per monomer of PET is 192, we see that in the absence of chain-folding ($\bar{n}=0$), the non-crystalline fraction of semicrystalline PET must behave as a highly cross-linked rubber in the plateau region (with only about five monomers per tie-segment). But the effective cross-link density (and hence the lengths of tie-segments) is critically dependent on the degree of chain-folding, decreasing with increasing $\bar{n}$.

Consider first the effects of increasing the *time* of thermal pre-treatment on the magnitude of the α'-relaxation. *Figure 12* shows that the height f_i of the plateau in f, and hence by implication the plateau modulus G_i, increases with time t_p. Structural measurements reviewed in the previous section showed an increase in density, and only a slight increase in L, with increasing t_p. Thus the increase in G_i is consistent with increasing crystallinity causing (a) an increase in the proportion of relatively rigid crystalline material, and (b) an increase in cross-linking of the non-crystalline fraction (see equation (25)) and hence in its contribution to G_i.

Now consider the quite different effect of increasing the *temperature* of heat-treatment. *Figure 11* shows clearly that the plateau height f_i, and hence G_i, *fall* with increasing T_p from 200°C to 240°C. At first sight this appears paradoxical, because increasing T_p is also associated with an increase in crystallinity. The difference between crystallinity introduced by increasing t_p and that introduced by increasing T_p must lie in the detail of the morphology. The analysis given above shows clearly the sensitivity of v to the degree of chain-folding. It is well established that a pronounced increase in chain-folding occurs when drawn PET is heat-treated at temperatures in the region of 200°C and above[10,70]. The increase in number of folds per molecule, $\bar{n}$, would decrease the effective cross-link density of the non-crystalline fraction. There may be a further contribution to a fall in v from crystal thickening (increasing long period L (equation (25))), which takes place in the same temperature region (*Figure 19*). These effects must combine to produce a reduction in modulus of the rubbery non-crystalline fraction, which is large enough to outweigh the effects of the increase in degree of crystallinity, and results in a net reduction in the plateau modulus G_i.

A similar conclusion, that constraint on the non-crystalline fraction of PET is reduced by high-temperature heat-treatment was arrived at from qualitative considerations in the early work of Illers and Breuer[32]. It was used by them to explain the fall in temperature of the α-relaxation (glass transition) with increasing annealing temperature beyond 150°C. It has been invoked also to explain the increase in dye uptake that occurs in PET fibres with increasing annealing temperature beyond 190°C (ref. 38).

CONCLUSIONS

The major results of the present work may be summarized as follows.

(1) There exists a high-temperature mechanical relaxation in semicrystalline PET, located between the glass transition and melting regions. It has been named here the α'-relaxation.

(2) Although overlapping the temperature range where melting/crystallization are likely to occur, the α'-relaxation appears not to involve these directly.

(3) The mechanism of the α'-relaxation is probably entanglement slippage, as occurs in non-crystalline uncrosslinked polymers of sufficiently high molecular weight.

(4) The time/temperature position of the α'-relaxation is highly sensitive to prior thermomechanical history. The relaxation is completely overlapped by the glass transition in as-drawn PET, but emerges as a well-defined separate process on heat-treatment. The molecular motion involved appears also to limit the rate of microstructural evolution during heat-treatment. As the microstructure evolves, the dominant relaxation time lengthens until it approximately equals the heat-treatment time made available.

(5) The magnitude of the α'-relaxation depends on the stiffening action of crystalline regions, acting both as inert reinforcing filler particles and also as cross-link sites for non-crystalline molecular segments. A surprising feature, the reduction in relaxation magnitude with increasing pre-setting temperature at 200°C and beyond, can be explained as being due to a reduction in the effective cross-link density contributed by crystals, because of increasing chain-folding and crystal thickening.

The practical significance of the α'-relaxation is that it occurs in the temperature region employed in numerous forming processes. It is clear that, for rapid forming, it is necessary to keep the dominant relaxation times of the α'-relaxation as short as possible at the forming temperature. The implication is that forming should always be effected at temperatures above those of previous heat-treatments. This, of course, is a well-known empirical rule widely applied in practice. We believe, however, that the present work provides a new understanding of its physical basis. It also offers the hope of a more quantitative approach being applied to design of processes and materials for forming, via the time/temperature relation of the α'relaxation and its manipulation by variation of the prior thermomechanical history.

ACKNOWLEDGEMENTS

The experiments described were made in the Department of Textile Technology, UMIST, Manchester. The authors are grateful to Professor J. W. S. Hearle for his interest and encouragement in the work. The measurement of intrinsic viscosity was kindly made by Mr Miaolin Hou at the Textile Research Institute, Princeton, USA. Financial support was received from the Science and Engineering Research Council and ICI Fibres.

APPENDIX

Model for calculating the cross-linking effect of crystals

Consider the situation sketched in *Figure 4a*, where crystals provide effective cross-link points for the non-crystalline matrix. We wish to calculate the number, v, of intercrystalline tie-segments per unit volume of non-crystalline polymer. We first need to make two resaonable assumptions to make the problem tractable: (1) assume that every molecule is incorporated into at least one crystal; (2) assume that all chain-ends are located in the non-crystalline fraction. A further simplification is helpful: we neglect any variations in crystal thickness.

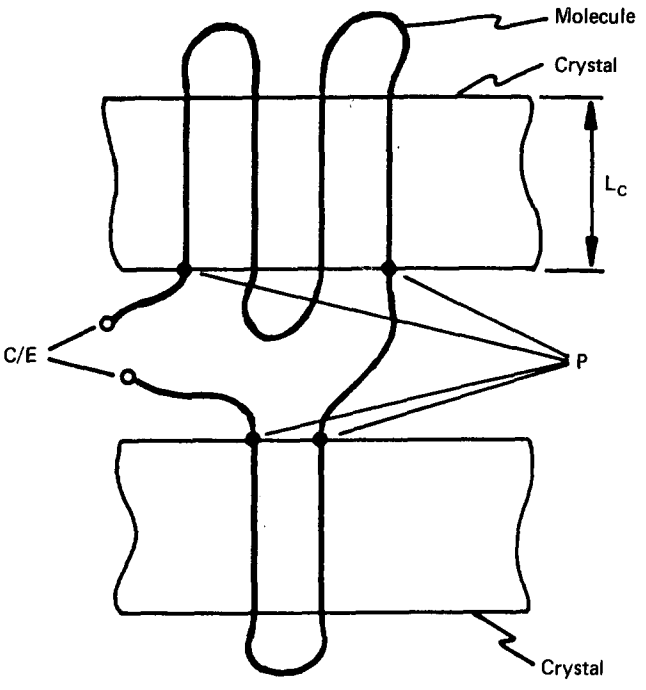

Figure 26 Sketch showing tie-segment linking two crystals. *Potential* tie-segment pinning points are labelled P. Chain-ends are labelledC/E. Two chain-ends remove one tie-segment

Consider the sketch in *Figure 26*. It is clear that every intercrystalline tie-segment *requires* two pinning points, as marked P. It is also clear that every incorporation of a molecule into a crystal *provides* two potential pinning points. Therefore, the number of potential tie-segments created is equal to the number of molecular incorporations in crystals. Moreover, the mean volume occupied in any one crystal by one molecule is simply $L_c A_0(\bar{n}+1)$, where $\bar{n}$ is the mean number of chain-folds per molecule per crystal, and A_0 is the cross-sectional area of the PET unit cell perpendicular to the molecular axis. Hence, ignoring the presence of chain-ends the number of tie-segments per unit volume of crystal is

$$\frac{1}{L_c A_0(\bar{n}+1)} \tag{A1}$$

The crystal thickness L_c is difficult to establish directly in PET. It is convenient, therefore, to approximate it from the long period L by using the expression

$$L_c = \chi_v L \tag{A2}$$

which applies to the idealized structure sketched in *Figure 8c*, where the entire specimen consists of stacks of alternating crystalline and non-crystalline layers. From equations (A1) and (A2) we find the total number of tie-segments per unit volume of non-crystalline polymer

$$\nu = \frac{1}{(1-\chi_v)LA_0(\bar{n}+1)} \text{ (ignoring chain ends)} \tag{A3}$$

The effect of introducing chain-ends is to remove some tie-segments, to become cilia instead (*Figure 26*) (assumption 1 above). Each molecule present contributes two chain-ends to the non-crystalline fraction (assumption 2 above), and two chain-ends remove one potential tie-segment. Thus ν is reduced from the value given in equation (A3) by a number equal to the total number of molecules present, expressed *per unit volume of non-crystalline polymer*. This is $\rho N_0/\bar{M}_n(1-\chi_v)$ where N_0 is Avogadro's number and $\bar{M}_n$ the number-average molecular weight. The chain-end-corrected density of tie-segments then becomes

$$\nu = \frac{1}{(1-\chi_v)}\left[\frac{1}{LA_0(\bar{n}+1)} - \frac{\rho N_0}{\bar{M}_n}\right] \tag{A4}$$

If the contributions of chain-folds and cilia to the mass of the non-crystalline fraction are neglected, the number-average tie-segment molecular weight $\bar{M}_t$ can be estimated from

$$\bar{M}_t \simeq \frac{\rho N_0}{\nu} \tag{A5}$$

In practice, this will be an overestimate, because some of the mass resides in chain-ends and cilia.

REFERENCES

1 Statton, W. O. and Goddard, G. M. *J. Appl. Phys.* 1957, **28**, 1111
2 Kilian, H. G., Kalboth, H. and Jenkel, E. *Kolloid-Z. Z. Polym.* 1960, **172**, 166
3 Heffelfinger, C. J. and Schmidt, P. G. *J. Appl. Polym. Sci.* 1965, **9**, 2661
4 Dismore, P. F. and Statton, W. O. *J. Polym. Sci.* 1966, **C13**, 133
5 Armediades, C. D., Kuriyama, I., Roe, J. M. and Baer, A. E. *J. Macromol. Sci. Phys.* 1967, **B1**, 777
6 Koenig, J. L. and Hannon, M. J. *J. Macromol. Sci. Phys.* 1967, **B1**, 119
7 Yeh, G. S. and Geil, P. H. *J. Macromol. Sci. Phys.* 1967, **B1**, 251
8 Bell, J. P. and Murayama, T. *J. Polym. Sci. A-2* 1969, **7**, 1059
9 Dumbleton, J. H. *J. Polym. Sci. A-2* 1969, **7**, 667
10 Statton, W. O., Koenig, J. L. and Hannon, M. J. *J. Appl. Phys.* 1970, **41**, 4290
11 Konrad, G. and Zachmann, H. G. *Kolloid. Z. Z. Polym.* 1971, **247**, 851
12 Dumbleton, J. H., Bell, J. P. and Murayama, T. *J. Appl. Polym. Sci.* 1972, **12**, 2491
13 Spruiell, J. E., McCord, D. E. and Beuerlein, R. A. *Trans. Soc. Rheol.* 1972, **16**, 535
14 Prevorsek, D. C., Tirpak, G. A., Harget, P. J. and Reimschuessel, A. C. *J. Macromol. Sci. Phys.* 1974, **9**, 733
15 Samuels, R. J. 'Structured Polymer Properties', Wiley, New York, 1974
16 Smith, F. S. and Steward, R. D. *Polymer* 1974, **15**, 283
17 Fakirov, S., Fischer, E. W. and Schmidt, G. F. *Macromol. Chem.* 1975, **176**, 2459
18 Bhatt, G. M. and Bell, J. P. *J. Polym. Sci. A-2* 1976, **14**, 575
19 Fischer, E. W. and Fakirov, S. F. *J. Mater. Sci.* 1976, **11**, 1041
20 Groeninckx, G. H., Bergmans, H. and Smets, G. *J. Polym. Sci. A-2* 1976, **14**, 591
21 Biangardi, H. J. and Zachmann, H. G. *J. Polym. Sci.* 1977, **C58**, 169
22 Eiko, I., Yamamato, K. and Kobayashi, Y. *Polymer* 1978, **19**, 39
23 Hindeleh, A. M. and Johnson, D. J. *Polymer* 1978, **19**, 27
24 Huisman, R. and Heuvel, M. M. *J. Appl. Polym. Sci.* 1978, **22**, 943
25 Gupta, V. B. and Kumar, S. *J. Appl. Polym. Sci.* 1981, **26**, 1865
26 Fontaine, F., Ledent, J., Groeninckx, G. and Reynaers, H. *Polymer* 1982, **23**, 185
27 Kawaguchi, T. *J. Polym. Sci.* 1958, **32**, 417
28 Farrow, G., McIntosh, J. and Ward, I. M. *Makromol. Chem.* 1960, **38**, 147
29 Kline, D. E. and Sauer, J. A. *Polymer* 1961, **2**, 401
30 Meredith, R. and Hsu Bay-Sung, *J. Polym. Sci.* 1962, **61**, 271
31 Takayanagi, M., Yoshino, M. and Minami, S. *J. Polym. Sci.* 1962, **61**, 171
32 Illers, K. H. and Breuer, H. *J. Colloid Sci.* 1963, **18**, 1

33 Pinnock, P. R. and Ward, I. M. *Proc. Phys. Soc.* 1963, **81**, 260
34 Pinnock, P. R. and Ward, I. M. *Polymer* 1966, **7**, 255
35 Dumbleton, J. H. and Murayama, T. *Kolloid Z. Z. Polym.* 1967, **220**, 41
36 Dumbleton, J. H. *Polymer* 1969, **10**, 539
37 Murayama, T. 'Dynamic Mechanical Analysis of Polymeric Materials', Elsevier, Amsterdam, 1978
38 Valk, G., Jellinek, G. and Schröder, U. *Text. Res. J.* 1980, **50**, 46
39 Gupta, V. B. and Kumar, S. *J. Appl. Polym. Sci.* 1981, **26**, 1877
40 Idem, ibid., 1885
41 Idem, ibid., 1897
42 Buckley, C. P. and McCrum, N. G. *J. Polym. Sci. A*-2 1971, **9**, 369
43 Lunn, A. C., Lee, B-L. and Yannas, I. V. *Polym. Eng. Sci.* 1974, **14**, 610
44 Shishoo, R. and Bergh, K. M. *Text. Res. J.* 1977, **47**, 56
45 Buckley, C. P., Hearle, J. W. S. and Mandal, R. *J. Text. Inst.* 1985, **76**, 264
46 Arghyros, S. and Backer, S. *Text. Res. J.* 1982, **52**, 295
47 Chapman, B. M. *J. Appl. Polym. Sci.* 1974, **18**, 3523
48 Denby, E. F. *Rheol. Acta.* 1975, **14**, 591
49 Chapman, B. M. *Text. Res. J.* 1976, **46**, 113
50 McCrum, N. G., Read, B. E. and Williams, G. 'Anaelastic and Dielectric Effects in Polymeric Solids', John Wiley and Sons, London, 1967
51 Ward, I. M. *Polymer* 1964, **5**, 59
52 Morland, L. W. and Lee, E. H. *Trans. Soc. Rheol.* 1960, **4**, 233
53 Alfrey, T. and Doty, P. *J. Appl. Phys.* 1945, **16**, 700
54 Hearle, J. W. S. in 'The Setting of Fibres and Fabrics' (Eds. J. W. S. Hearle and L. W. C. Miles), Merrow Publishing Co., Watford 1971, Ch. 1 and 5
55 Ravens, D. A. S. and Ward, I. M. *Trans. Farad. Soc.* 1961, **57**, 150
56 Dauberry, R. de P., Bunn, C. W. and Brown, C. J. *Proc. Roy. Soc. Lond.* 1954, **A226**, 531
57 Farrow, G. and Ward, I. M. *Polymer* 1961, **2**, 341
58 Hall, I. H. and Toy, M. in 'Structure of Crystalline Polymers' (Ed. I. H. Hall), Elsevier Applied Science Publishers, London, 1984
59 Salem, D. R. PhD thesis, University of Manchester, 1982
60 Roberts, R. C. *Polym. Lett.* 1970, **8**, 381
61 Holdsworth, P. J. and Turner-Jones, A. *Polymer* 1971, **12**, 195
62 Sweet, G. E. and Bell, J. P. *J. Polym. Sci. A*-2, 1972, **10**, 1273
63 Groeninckx, G., Reyaers, H., Berghmans, H. and Smets, G. *J. Polym. Sci., Polym. Phys. Edn.* 1980, **18**, 1311
64 Idem, ibid., 1325
65 Berndt, H.-J. and Bossman, A. *Polymer* 1976, **17**, 241
66 Weighmann, H. D., Scott, M. G. and Ribnick, S. *Text. Res. J.* 1977, **47**, 761
67 Petrie, S. E. B. *J. Macromol. Sci., Phys.* 1976, **B12**, 225
68 Ferry, J. D. 'Viscoelastic Properties of Polymers', 3rd Edn., John Wiley and Sons, New York, 1980
69 Hoffman, J. D., Williams, G. and Passaglia, E. A. *J. Polym. Sci.* 1966, **C14**, 173
70 Wilson, M. P. W. *Polymer* 1974, **15**, 277